

GENESIS-V2: Inferring Unordered Object Representations without Iterative Refinement

Martin Engelcke*, Oiwi Parker Jones, and Ingmar Posner

Applied AI Lab, University of Oxford, UK
 {martin, oiwi, ingmar}@robots.ox.ac.uk

Abstract

Advances in unsupervised learning of object-representations have culminated in the development of a broad range of methods for unsupervised object segmentation and interpretable object-centric scene generation. These methods, however, are limited to simulated and real-world datasets with limited visual complexity. Moreover, object representations are often inferred using RNNs which do not scale well to large images or iterative refinement which avoids imposing an unnatural ordering on objects in an image but requires the *a priori* initialisation of a fixed number of object representations. In contrast to established paradigms, this work proposes an embedding-based approach in which embeddings of pixels are clustered in a differentiable fashion using a stochastic stick-breaking process. Similar to iterative refinement, this clustering procedure also leads to randomly ordered object representations, but without the need of initialising a fixed number of clusters *a priori*. This is used to develop a new model, GENESIS-V2, which can infer a variable number of object representations without using RNNs or iterative refinement. We show that GENESIS-V2 performs strongly in comparison to recent baselines in terms of unsupervised image segmentation and object-centric scene generation on established synthetic datasets as well as more complex real-world datasets.

1 Introduction

Reasoning about discrete objects in an environment is foundational to how agents perceive their surroundings and act in it. For example, autonomous vehicles need to identify and respond to other road users (e.g. [1, 2]) and robotic manipulation tasks involve grasping and pushing individual objects (e.g. [3]). While supervised methods can identify selected objects (e.g. [4, 5]), it is intractable to manually collect labels for every possible object category. Furthermore, we often desire the ability to predict, or *imagine*, how a collection of objects might behave (e.g. [6]). A range of works have thus explored unsupervised segmentation and object-centric generation in recent years (e.g. [7–36]). These models are often formulated as variational autoencoders (VAEs) [37, 38] which allow the joint learning of inference and generation networks to identify objects in images and to generate scenes in an object-centric fashion (e.g. [15, 17, 28]).

Moreover, such models require a differentiable mechanism for separating objects in an image. While some works use spatial transformer networks (STNs) [39] to process crops that contain objects (e.g. [7–15]), others directly predict pixel-wise instance segmentation masks (e.g. [16–27]). The latter avoids the use of fixed-size sampling grids which are ill-suited for objects of varying size. Instead, object representations are inferred either by iteratively refining a set of randomly initialised representations (e.g. [19–24]) or by using a recurrent neural networks (RNN) (e.g. [16–18]). One particularly interesting model of the latter category is GENESIS [17] can perform both scene segmentation and generation by capturing relationships between objects with an autoregressive prior.

*Now affiliated with Google DeepMind.

As noted in Novotny et al. [40], however, using RNNs for instance segmentation requires processing high-dimensional inputs in a sequential fashion which is computationally expensive and does not scale well to large images with potentially many objects. We also posit that recurrent inference is not only problematic from a computational point of view, but that it can also inhibit the learning of object representations by imposing an unnatural *ordering* on objects. In particular, we argue that this leads to different *object slots* receiving gradients of varying magnitude which provides a possible explanation for models collapsing to a single object slot during training, unless the flexibility of the model is restricted (see [18]). While iterative refinement instead infers unordered object representations, it requires the *a priori* initialisation of a fixed number of object slots even though the number of objects in an image is unknown.

In contrast, our work takes inspiration from the literature on supervised instance segmentation and adopts an *instance colouring* approach (e.g. [40–43]) in which pixel-wise embeddings—or colours—are clustered into attention masks. Typically, either a supervised learning signal is used to obtain cluster seeds (e.g. [40, 41]) or clustering is performed as a non-differentiable post-processing operation (e.g. [42, 43]). Neither of these approaches is suitable for unsupervised, end-to-end learning of segmentation masks. We hence develop an *instance colouring stick-breaking process* (IC-SBP) to cluster embeddings in a differentiable fashion. This is achieved by stochastically sampling cluster seeds from the pixel embeddings to perform a soft grouping of the embeddings into a set of randomly ordered attention masks. It is therefore possible to infer object representations both without imposing a fixed ordering or performing iterative refinement.

Inspired by GENESIS [17], we leverage the IC-SBP to develop GENESIS-V2, a novel model that learns to segment objects in images without supervision and that uses an autoregressive prior to generate scenes in an interpretable, object-centric fashion. GENESIS-V2 is comprehensively benchmarked against recent prior art [16, 17, 24] on established synthetic datasets—ObjectsRoom [44] and ShapeStacks [45]—where it performs strongly in comparison to several recent baselines. We also evaluate GENESIS-V2 on more challenging real-world images from the Sketchy [46] and the MIT-Princeton Amazon Picking Challenge (APC) 2016 Object Segmentation datasets [47], where it also achieves promising results. Code and pre-trained models are available at <https://github.com/applied-ai-lab/genesis>.

2 Related Work

Unsupervised models for learning object representations are typically formulated either as autoencoders (e.g. [7–10, 12–28]) or generative adversarial networks (GANs) (e.g. [29–36]). Typical GANs are able to generate images, but lack an associated inference mechanism and often suffer from training instabilities (see e.g. [48, 49]). A comprehensive review and discussion of the subject is provided in Greff et al. [50].

In order to infer object representations, STNs [39] can explicitly disentangle object location by cropping out a rectangular region from an input, allowing object appearance to be modelled in a canonical pose (e.g. [7–10, 12–15]). This operation, however, relies on a fixed-size sampling grid which is not well-suited if objects vary broadly in terms of scale. In addition, gradients are usually obtained via bi-linear interpolation and are therefore limited to the extent of the sampling grid which can impede training: for example, if the sampling grid does not overlap with any object, then its location cannot be updated in a meaningful way. In contrast, purely segmentation based approaches [16–27]) often use RNNs (e.g. [16–18]) or iterative refinement (e.g. [19–24]) to infer object representations from an image. Other works either use a fixed number of slots [25, 26] or group pixels in a non-differentiable fashion [27]. RNN based models need to learn a fixed strategy that sequentially attends to different regions in an image, but this imposes an unnatural ordering on objects in an image. Avoiding such a fixed ordering leads to a *routing problem*. One way to address this is by randomly initialising a set of object representations and iteratively refining them. More broadly, this is also related to Deep Set Prediction Networks [51], where a set is iteratively refined in a gradient-based fashion. The main disadvantage of iterative refinement is that it is necessary to initialise a fixed number of clusters *a priori*, even though ideally we would like the number of clusters to be input-dependent. This is directly facilitated by the proposed IC-SBP. The IC-SBP and GENESIS-V2 are in this respect also related to the Stick-Breaking VAE [52] which uses a stochastic number of latent variables, but does not attempt to explicitly capture the object-based structure of visual scenes.

Unlike some other works which learn unsupervised object representations from video sequences (e.g. [13, 14]), our work considers the more difficult task of learning such representations from individual images alone. GENESIS-V2 is most directly related to GENESIS [17] and SLOT-ATTENTION [24]. Like GENESIS, the model is formulated as a VAE to perform both object segmentation and object-centric scene generation, whereby the latter is facilitated by an autoregressive prior. Similar to SLOT-ATTENTION, the model uses a shared convolutional encoder to extract a feature map from which features are pooled via an attention mechanism to infer object representations with a random ordering. In contrast to SLOT-ATTENTION, however, the attention masks are obtained with a parameter-free clustering algorithm that does not require iterative refinement or a predefined number of clusters. Both GENESIS and SLOT-ATTENTION are only evaluated on synthetic datasets. In this work, we use synthetic datasets for quantitative benchmarking, but we also perform experiments on two more challenging real-world datasets.

3 GENESIS-V2

An image \mathbf{x} of height H , width W , with C channels, and pixel values in the interval $[0, 1]$ is considered to be a three-dimensional tensor $\mathbf{x} \in [0, 1]^{H \times W \times C}$. This work is only concerned with RGB images where $C = 3$, but other input modalities with a different number of channels could also be considered. Assigning individual pixels to object-like scene components can be formulated as obtaining a set of *object masks* $\pi \in [0, 1]^{H \times W \times K}$ with $\sum_k \pi_{i,j,k} = 1$ for all pixel coordinate tuples (i, j) in an image, where K is the number of scene components. Inspired by prior works (e.g. [16, 22]) and identical to Engelcke et al. [17], this is achieved by modelling the image likelihood $p_\theta(\mathbf{x} | \mathbf{z}_{1:K})$ as an SGMM of the form

$$\log p_\theta(\mathbf{x} | \mathbf{z}_{1:K}) = \sum_{i=1}^H \sum_{j=1}^W \sum_{c=1}^C \log \left(\sum_{k=1}^K \pi_{i,j,k}(\mathbf{z}_{1:K}) \mathcal{N}(\mu_{i,j,c}(\mathbf{z}_k), \sigma_x^2) \right). \quad (1)$$

The parameters θ of the model are learned σ_x is a fixed standard deviation that is shared across object slots. The summation in Equation (1) implies that the likelihood is *permutation-invariant* to the order of the object representations $\mathbf{z}_{1:K}$ (see e.g. [53, 54]) provided that $\pi_{i,j,k}(\mathbf{z}_{1:K})$ is also permutation-invariant. This allows the generative model to accommodate for a variable number of object representations.

To segment objects in images and to generate synthetic images in an object-centric fashion requires the formulation of appropriate inference and generative models, i.e. $q_\phi(\mathbf{z}_{1:K} | \mathbf{x})$ and $p_\theta(\mathbf{x} | \mathbf{z}_{1:K}) p_\theta(\mathbf{z}_{1:K})$, respectively, where ϕ are also learnable parameters. In the generative model, it is necessary to model relationships between object representations to facilitate the generation of coherent scenes. Inspired by GENESIS [17], this is facilitated by an autoregressive prior

$$p_\theta(\mathbf{z}_{1:K}) = \prod_{k=1}^K p_\theta(\mathbf{z}_k | \mathbf{z}_{1:k-1}). \quad (2)$$

GENESIS uses two sets of latent variables to encode object masks and appearances separately. In contrast, GENESIS-V2 uses one set of latent variables $\mathbf{z}_{1:K}$ to encode both, which increases parameter sharing. The graphical model of GENESIS-V2 is shown next to related models in Appendix A.

While GENESIS relies on a recurrent mechanism in the inference model to predict segmentation masks, GENESIS-V2 instead infers latent variables without imposing a fixed ordering and assumes object latents $\mathbf{z}_{1:K}$ to be conditionally independent given an input image \mathbf{x} , i.e., $q_\phi(\mathbf{z}_{1:K} | \mathbf{x}) = \prod_k q_\phi(\mathbf{z}_k | \mathbf{x})$. Specifically, GENESIS-V2 first extracts an encoding with a deterministic UNet backbone. This encoding is used to predict a map of *semi-convolutional* pixel embeddings $\zeta \in \mathbb{R}^{H \times W \times D_\zeta}$ (see [40]). Semi-convolutional embeddings are introduced in Novotny et al. [40] to facilitate the prediction of unique embeddings for multiple objects of identical appearance. The embeddings are computed by performing an element-wise addition of pixel coordinates to two dimensions of the embeddings. In this work, we let the pixel coordinates be in the interval $[-1, 1]$ relative to the image centre. Subsequently, the IC-SBP converts the embeddings into a set of normalised *attention masks* $\mathbf{m} \in [0, 1]^{H \times W \times K}$ with $\sum_k m_{i,j,k} = 1$ via a distance kernel ψ . The spatial structure of the embeddings should induce the attention masks to be spatially localised, but this is not a hard constraint. In addition, we derive principled initialisations for the scaling-factor of different IC-SBP distance kernels ψ in Section 3.2.

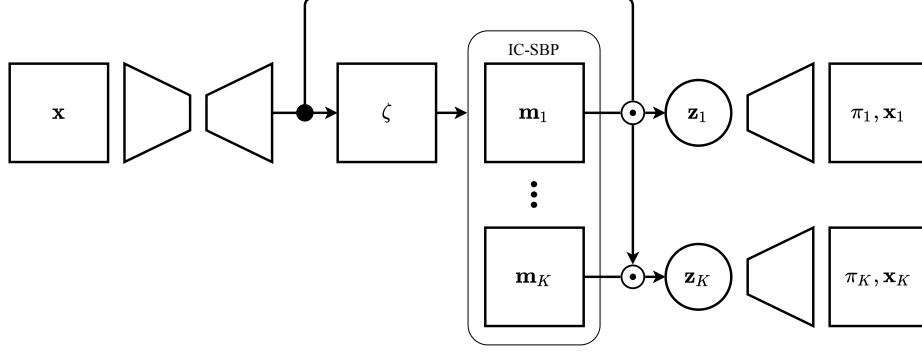


Figure 1: GENESIS-v2 overview. The image \mathbf{x} is passed into a deterministic backbone. The resulting encoding is used to compute the pixel embeddings ζ which are clustered into attention masks $\mathbf{m}_{1:K}$ by the IC-SBP. Features are pooled according to these attention masks to infer the object latents $\mathbf{z}_{1:K}$. These are decoded into the object masks $\pi_{1:K}$ and reconstructed components $\mathbf{x}_{1:K}$.

Inspired by Locatello et al. [24], GENESIS-v2 uses the attention masks $\mathbf{m}_{1:K}$ to pool a feature vector for each scene component from the deterministic image encoding. A set of object latents $\mathbf{z}_{1:K}$ is then computed from these feature vectors. This set of latents is decoded in parallel to compute the statistics of the SGMM in Equation (1). The object masks π are normalised with a softmax operator. The inference and generation models can be jointly trained as a VAE as illustrated in Figure 1. Further architecture details are described in Appendix B.

3.1 Instance Colouring Stick-Breaking Process

The IC-SBP is a stochastic, differentiable algorithm that clusters pixel embeddings $\zeta \in \mathbb{R}^{H \times W \times D_\zeta}$ into a variable number of soft attention masks $\mathbf{m} \in [0, 1]^{H \times W \times K}$. Intuitively, this is achieved by (1) sampling the location (i, j) of a pixel that has not been assigned to a cluster yet, (2) creating a soft or hard cluster according to the distance of the embedding $\zeta_{i,j}$ at the selected pixel location to all other pixel embeddings according to a kernel ψ , and (3) repeating the previous two steps until all pixels are explained or some form of stopping condition is reached. Crucially, the stochastic selection of pixel embeddings as *cluster seeds* leads to a set of *randomly ordered soft clusters*. Due to its conceptual similarity, the method derives its name from more formal stick-breaking process formulations as can, e.g., be found in Yuan et al. [11] or Nalisnick and Smyth [52].

The IC-SBP is described more formally in Algorithm 1. Specifically and inspired by Burgess et al. [16], a *scope* $\mathbf{s} \in [0, 1]^{H \times W}$ is initialised to a matrix of ones $\mathbb{1}^{H \times W}$ to track the degree to which pixels have been assigned to clusters. In addition, a matrix of *seed scores* is created once by sampling from a uniform distribution $\mathbf{c} \sim U(0, 1) \in \mathbb{R}^{H \times W}$ to perform the stochastic selection of pixel embeddings. At each iteration, a single embedding vector $\zeta_{i,j}$ is selected at the spatial location (i, j) which corresponds to the argmax of the element-wise multiplication of the seed scores and the current scope. This ensures that cluster seeds are sampled from pixel embeddings that have not yet been assigned to clusters. An alpha mask $\alpha_k \in [0, 1]^{H \times W}$ is computed as the distance between the cluster seed embedding $\zeta_{i,j}$ and all individual pixel embeddings according to a distance kernel ψ . The output of the kernel ψ is one if two embeddings are identical and decreases to zero as the distance between a pair of embeddings increases. The associated attention mask \mathbf{m}_k is obtained by the element-wise multiplication of the alpha masks by the current scope to ensure that the final set of attention masks is normalised. The scope is then updated by an element-wise multiplication with the complement of the alpha masks. This process is repeated until a stopping condition is satisfied, at which point the final scope is added as an additional mask to explain any remaining pixels.

In this work, we restrict ourselves to soft cluster assignment, leading to continuous attention masks with values in $\mathbf{m}_k \in [0, 1]^{H \times W}$. Unless the attention masks take binary values, several executions of the algorithm will lead to slightly different masks for individual objects. If the mask values are discrete and exactly equal to zero or one, however, then the set of cluster seeds and the set of attention masks are uniquely defined apart from their ordering. This can be inferred from the fact that if at each step of the IC-SBP produces a discrete mask, then embeddings associated with this mask cannot

Algorithm 1: Instance Colouring Stick-Breaking Process

Input: embeddings $\zeta \in \mathbb{R}^{H \times W \times D_\zeta}$ **Output:** masks $\mathbf{m}_{1:K}$ with $\mathbf{m}_k \in [0, 1]^{H \times W}$ **Initialise:** masks $\mathbf{m} = \emptyset$, scope $\mathbf{s} = \mathbb{1}^{H \times W}$, seed scores $\mathbf{c} \sim U(0, 1) \in \mathbb{R}^{H \times W}$ **while** *not* $\text{StopCondition}(\mathbf{m})$ **do** $\quad \mathbf{i}, \mathbf{j} = \text{argmax}(\mathbf{s} \odot \mathbf{c});$
 $\quad \alpha = \text{DistanceKernel}(\zeta, \zeta_{\mathbf{i}, \mathbf{j}});$
 $\quad \mathbf{m.append}(\mathbf{s} \odot \alpha);$
 $\quad \mathbf{s} = \mathbf{s} \odot (1 - \alpha);$ **end** $\mathbf{m.append}(\mathbf{s})$

be sampled as cluster seeds later on due to the masking of the seed scores by the scope. A different cluster with an associated discrete mask is therefore created at every step until all embeddings are uniquely clustered. Another interesting modification would be to use continuous masks while making the output of the IC-SBP *permutation-equivariant* with respect to the ordering of the cluster seeds. This could be achieved either by directly using the cluster seeds for downstream computations or by separating the mask normalisation from the stochastic seed selection. While the SBP formulation facilitates the selection of a diverse set of cluster seeds, the masks could be normalised separately after the cluster seeds are selected by using a softmax operation, for example. An investigation of these ideas is left for future work.

In contrast to GENESIS, the stochastic ordering of the masks implies that it is not possible for GENESIS-V2 to learn a fixed sequential decomposition strategy. While this does not strictly apply to the last mask which is set equal to the remaining scope, we find empirically that models learn a strategy where the final scope is either largely unused or where it corresponds to a generic background cluster with foreground objects remaining unordered as desired. Unlike as in iterative refinement where a fixed number of clusters needs to be initialised *a priori*, the IC-SBP can infer a variable number of object representations by using a heuristic that considers the current set of attention masks at every iteration in Algorithm 1. While we use a fixed number of K masks during training for efficient parallelism on GPU accelerators, we demonstrate that a flexible number of masks can be extracted at test time with minimal impact on segmentation performance.

3.2 Kernel Initialisation with Semi-Convolutional Embeddings

For semi-convolutional embeddings to be similar according to a distance kernel ψ , the model needs to learn to compensate for the addition of the relative pixel coordinates. It can achieve this by predicting a *delta vector* for each embedding to a specific pixel location, for example to the centre of the object that the embedding belongs to. A corollary of this is that if embeddings are equal to the relative pixel coordinates with the other dimensions being zero, then clustering embeddings based on their relative distances results in “blob-like”, spatially localised masks. In this work, we make use of this property to derive a meaningful initialisation for free parameters in the distance kernel ψ of the IC-SBP. Established candidates for ψ from the literature are the Gaussian ψ_G [40], Laplacian ψ_L [40], and Epanechnikov ψ_E kernels [55] with

$$\psi_G = \exp\left(-\frac{\|\mathbf{u}-\mathbf{v}\|^2}{\sigma_G}\right), \quad \psi_L = \exp\left(-\frac{\|\mathbf{u}-\mathbf{v}\|}{\sigma_L}\right), \quad \psi_E = \max\left(1 - \frac{\|\mathbf{u}-\mathbf{v}\|^2}{\sigma_E}, 0\right), \quad (3)$$

whereby \mathbf{u} and \mathbf{v} are two embeddings of equal dimension. Each kernel contains a scaling factor $\sigma_{\{G,L,E\}} \in \mathbb{R}^+$. By initialising the model at the beginning of training so that the embeddings are equal to the relative pixel coordinates with the other dimensions being zero, then $\sigma_{\{G,L,E\}}$ can be initialised so that the initial attention masks are similarly-sized circular patches. In particular, we initialise these scaling factors as

$$\sigma_G^{-1} = K \ln 2, \quad \sigma_L^{-1} = \sqrt{K} \ln 2, \quad \sigma_E^{-1} = K/2, \quad (4)$$

which is derived and illustrated in Appendix C. After initialisation, $\sigma_{\{G,L,E\}}$ is jointly optimised along with the other learnable parameters of the model as in Novotny et al. [40].

3.3 Training

Following Engelcke et al. [17], GENESIS-v2 is trained by minimising the GECO objective [56], which can be written as a loss function of the form

$$\mathcal{L}_g = \mathbb{E}_{q_\phi(\mathbf{z}|\mathbf{x})}[-\ln p_\theta(\mathbf{x}|\mathbf{z})] + \beta_g \cdot \text{KL}[q_\phi(\mathbf{z}|\mathbf{x}) \parallel p_\theta(\mathbf{z})]. \quad (5)$$

The relative weighting factor $\beta_g \in \mathbb{R}^+$ is updated at every training iteration separately from the model parameters according to

$$\beta_g = \beta_g \cdot e^{\eta(C-E)} \quad \text{with} \quad E = \alpha_g \cdot E + (1 - \alpha_g) \cdot \mathbb{E}_{q_\phi(\mathbf{z}|\mathbf{x})}[-\ln p_\theta(\mathbf{x}|\mathbf{z})]. \quad (6)$$

$E \in \mathbb{R}$ is an exponential moving average of the negative image log-likelihood, $\alpha_g \in [0, 1]$ is a momentum factor, $\eta \in \mathbb{R}^+$ is a step size hyperparameter, and $C \in \mathbb{R}$ is a target reconstruction error. Intuitively, the optimisation decreases the weighting of the KL (Kullback-Leibler) regularisation term as long as the reconstruction error is larger than the target C . The weighting of the KL term is increased again once the target is satisfied.

In some applications, a practitioner might only require segmentation masks in which case, so having to reconstruct the entire input would be rather inefficient. While we observed that the attention masks \mathbf{m} are correlated to the object masks π , they do not align as closely with object boundaries. We conjecture that this is a consequence of the large receptive field of the UNet backbone which spatially dilates information about objects. Consequently, we also conduct experiments with an additional auxiliary mask consistency loss that encourages attention masks \mathbf{m} and object masks π to be similar. This leads to a modified loss function of the form

$$\mathcal{L}'_g = E + \beta_g \cdot (\text{KL}[q_\phi(\mathbf{z}|\mathbf{x}) \parallel p_\theta(\mathbf{z})] + \text{KL}[\mathbf{m} \parallel \text{nograd}(\pi)]), \quad (7)$$

in which \mathbf{m} and π are interpreted as pixel-wise categorical distributions. Preliminary experiments indicated that stopping the gradient propagation through the object masks π helps to achieve segmentation quality comparable to using the original loss function in Equation (5).

4 Experiments

This section presents results on two simulated datasets—ObjectsRoom [44] and ShapeStacks [45]—as well as two real-world datasets—Sketchy [46] and APC [47]—which are described in Appendix D. GENESIS-v2 is compared against three recent baselines: GENESIS [17], MONET [16], and SLOT-ATTENTION [24]. Even though SLOT-ATTENTION is trained with a pure reconstruction objective and is not a generative model, it is an informative and strong baseline for unsupervised scene segmentation. The other models are trained with the GECO objective [56] following the protocol from Engelcke et al. [17] for comparability. We refer to MONET trained with GECO as MONET-G to avoid conflating the results with the original settings. Further training details are described in Appendix E.

Following prior works (e.g. [17, 18, 22, 24]), segmentation quality is quantified using the Adjusted Rand Index (ARI) [57] and the Mean Segmentation Covering (MSC). The MSC is derived from Arbelaez et al. [58] and described in detail in Engelcke et al. [17]. These are by default computed using pixels belonging to ground truth foreground objects (ARI-FG and MSC-FG). Similar to Greff et al. [22], these are averaged over 320 images from respective test sets. We also report the Evidence Lower Bound (ELBO) averaged over 320 test images as a measure how well the generative models are able to fit the data. Generation quality is measured using the Fréchet Inception Distance (FID) [59] which is computed from 10,000 samples and 10,000 test set images using the implementation from Seitzer [60]. When models are trained with multiple random seeds, we always show qualitative results for the seed that achieves the highest ARI-FG. In terms of the two real-world datasets, there are only ground truth segmentation masks available for the APC data, with the caveat that there is only a single foreground object per image. In this case, when computing the segmentation metrics from foreground pixels alone, the ARI-FG could be trivially maximised by assigning all image pixels to the same component and the MSC-FG would be equal to the largest IOU between the predicted masks and the foreground objects. When considering all pixels, the optimal solution for both metrics is to have exactly one set of pixels assigned to the foreground object and another set of pixels being assigned to the background. While acknowledging that segmenting the background as a single component is arguably not the only valid way of segmenting the background, we report the ARI and MSC using all pixels instead to develop a sense of how well foreground objects are separated from the background.

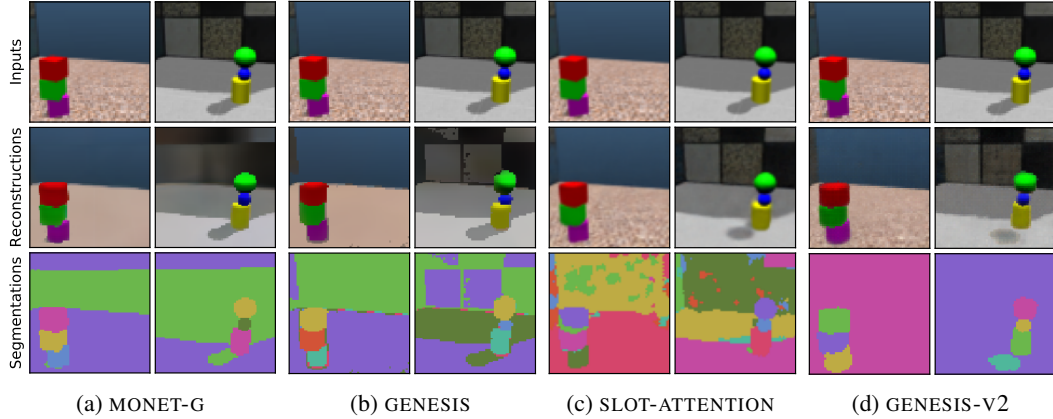


Figure 2: GENESIS-V2 learns better reconstructions and segmentations on ShapeStacks.

Table 1: Means and standard deviations of the segmentation metrics from three seeds. Bold values in the first half of the table indicate the best values for the generative models; bold values in the second half indicate any better values achieved by the additional non-generative baseline.

Model	Generative	ObjectsRoom		ShapeStacks	
		ARI-FG	MSC-FG	ARI-FG	MSC-FG
MONET-G	Yes	0.54±0.00	0.33±0.01	0.70±0.04	0.57±0.12
GENESIS	Yes	0.63±0.03	0.53±0.07	0.70±0.05	0.67±0.02
GENESIS-V2	Yes	0.85±0.01	0.59±0.01	0.81±0.01	0.67±0.01
SLOT-ATTENTION	No	0.79±0.02	0.64±0.13	0.76±0.01	0.70±0.05

4.1 Benchmarking in Simulation

Figure 2 shows qualitative results on ShapeStacks and additional qualitative results are included in Appendix F. GENESIS-V2 cleanly separates the foreground objects from the background and the reconstructions. Interestingly, GENESIS-V2 is the only model that segments the entire background as a single component. We conjecture that this behaviour is a consequence of the fact that the background structures are of finite variety. As a result, even when viewing only a fraction of the background, it is possible for the model to largely predict the appearance of the rest of the background. The KL regularisation during training encourages efficient compression of the inputs, which penalises redundant information between slots and might thus explain this behaviour. SLOT-ATTENTION is trained without KL regularisation and the decoders of MONET-G as well GENESIS are possibly not flexible enough to reconstruct the entire background as a single component (see Appendix B for architecture details).

In terms of quantitative performance, Table 1 summarises the segmentation results on ObjectsRoom and ShapeStacks. GENESIS-V2 outperforms the two generative baselines GENESIS and MONET-G across datasets on all metrics, showing that the IC-SBP is indeed suitable for learning object-centric representations. GENESIS-V2 outperforms the non-generative SLOT-ATTENTION baseline in terms of the ARI-FG on both datasets. SLOT-ATTENTION manages to achieve a better mean MSC-FG. The standard deviation of the MSC-FG values is much larger, though, which indicates training is not as stable. While the ARI-FG indicates the models ability to separate objects, it does not penalise the undersegmentation of objects (see [17]). The MSC-FG, in contrast, is an IOU based metric and sensitive to the exact segmentation masks. We conjecture that SLOT-ATTENTION manages to predict slightly more accurate segmentation masks given that it is trained on a pure reconstruction objective and without KL regularisation, thus leading to a slightly better mean MSC-FG. A set of ablations for GENESIS-V2 is also included in Appendix F.

Table 2: Means and standard deviations of the segmentation metrics from three seeds for GENESIS-V2 with a fixed or flexible number of object slots. Highlighting follows an analogous scheme as in Table 1.

Dataset	Training	Slots	Avg. $K \downarrow$	MAE \downarrow	ARI-FG \uparrow	MSC-FG \uparrow
ObjectsRoom	No mask loss	Fixed	7.0 \pm 0.0	3.3 \pm 0.0	0.85\pm0.01	0.59\pm0.01
		Flexible	5.0\pm0.9	1.7\pm0.9	0.84 \pm 0.01	0.51 \pm 0.10
ShapeStacks	No mask loss	Fixed	9.0 \pm 0.0	4.4 \pm 0.0	0.81\pm0.01	0.67\pm0.01
		Flexible	6.3\pm0.3	1.9\pm0.3	0.77 \pm 0.02	0.63 \pm 0.01
	With mask loss	Fixed	9.0 \pm 0.0	4.4 \pm 0.0	0.81\pm0.01	0.68\pm0.00
		Flexible	5.7\pm0.2	1.1\pm0.02	0.81\pm0.01	0.68\pm0.01

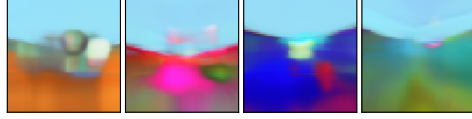
Table 3: Means and standard deviations of ELBO values and FID scores from three seeds.

Model	ObjectsRoom		ShapeStacks	
	ELBO \uparrow	FID \downarrow	ELBO \uparrow	FID \downarrow
MONET-G	-7217 \pm 19	205.7 \pm 7.6	-7268 \pm 19	197.8 \pm 5.2
GENESIS	-7023\pm2	62.8 \pm 2.5	-7082 \pm 15	186.8 \pm 18.0
SLOT-ATT.	—	—	—	—
GENESIS-V2	-7040 \pm 2	52.6\pm2.7	-7019\pm2	112.7\pm3.2

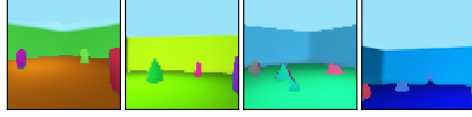
We also examine whether the IC-SBP can indeed be used to extract a variable number of object representations. This is done by terminating the IC-SBP according to a manual heuristic and setting the final mask to the remaining scope. Specifically, we terminate the IC-SBP when the sum of the current attention mask values is smaller than 70 pixels for ObjectsRoom and 20 pixels for ShapeStacks. A larger threshold is used for the former as the attention masks tend to be more dilated (see Appendix F). The average number of used slots, the Mean Absolute Error (MAE) to the ideal number of slots, and segmentation metrics are when using a fixed number and a variable number slots after training are summarised in Table 2. On both datasets, allowing for a flexible number requires fewer steps and achieves a smaller MAE. This is incurred, though, at a drop in segmentation performance. When training GENESIS-V2 with the auxiliary mask loss as in Equation (7) on ShapeStacks, the average number of steps and the MAE further decrease at no impact on the segmentation metrics. On ObjectsRoom, the auxiliary mask loss appeared to deteriorate the learning of good object segmentations and the associated results are therefore not included.

In terms of density estimation and scene generation, Table 3 summarises the ELBO values and FID scores for GENESIS-V2 and the baselines on ObjectsRoom and ShapeStacks.² GENESIS achieves a slightly better ELBO than GENESIS-V2 on ObjectsRoom, but GENESIS-V2 performs significantly better on ShapeStacks. We hypothesise that GENESIS benefits here from having a more flexible, autoregressive posterior than GENESIS-V2. Regarding scene generation, GENESIS-V2 consistently performs best with a particularly significant improvement on ShapeStacks. Results on ShapeStacks, however, are not as good as for ObjectsRoom, which is likely caused by the increased visual complexity of the images in the ShapeStacks dataset. Qualitative results for scene generation are shown in Figures 3 and 4. Both GENESIS and GENESIS-V2 produce reasonable samples after training on ObjectsRoom. For ShapeStacks, samples from GENESIS contain significant distortions. In comparison, samples from GENESIS-V2 are more realistic, but also still show room for improvement.

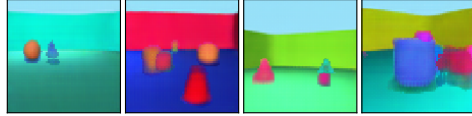
²Note that in contrast to the MONET-G training objective, the decoded mask distribution rather than the deterministic attention masks are used to compute the reconstruction likelihood in the ELBO calculation for MONET-G. The KL divergence between the two mask distributions as used in the training objective is not part of this ELBO calculation.



(a) MONET-G



(b) GENESIS

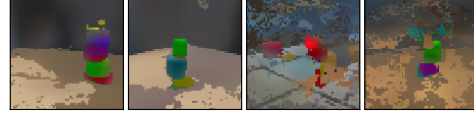


(c) GENESIS-V2

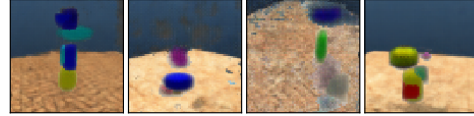
Figure 3: ObjectsRoom samples.



(a) MONET-G



(b) GENESIS



(c) GENESIS-V2

Figure 4: ShapeStacks samples.

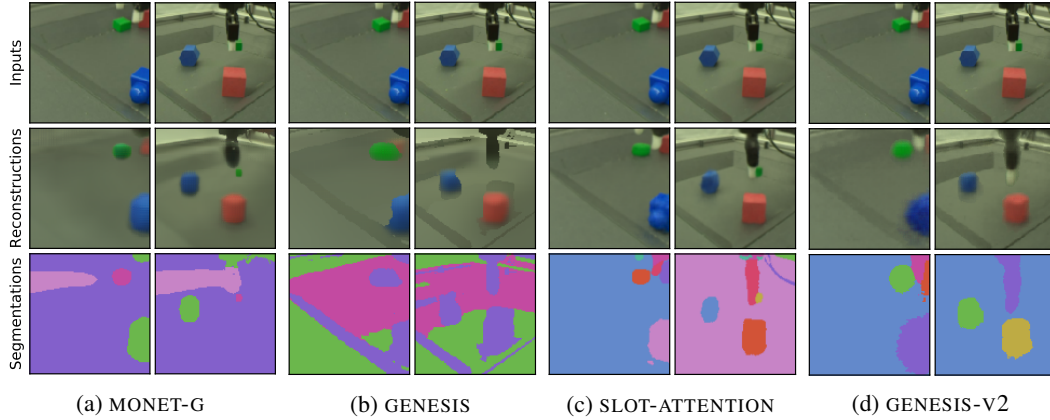


Figure 5: In contrast to MONET-G and GENESIS, GENESIS-V2 as well as SLOT-ATTENTION are able to learn reasonable object segmentations on the more challenging Sketchy dataset.

4.2 Real-World Applications

After validating GENESIS-V2 on two simulated datasets, this section presents experiments on the Sketchy [46] and APC datasets [47]; two significantly more challenging real-world datasets collected in the context of robot manipulation. Due to the long training time on these datasets, each model is only trained with a single random seed. While this makes it infeasible to draw statistically strong conclusions, the aim of this section is to provide an indication and early exploration of how these models fare on more complex real-world datasets. Reconstructions and segmentations after training GENESIS-V2 on Sketchy and APC are shown in Figures 5 and 6. For Sketchy, it can be seen that GENESIS-V2 and SLOT-ATTENTION disambiguate the individual foreground objects and the robot gripper fairly well. SLOT-ATTENTION produces slightly more accurate reconstructions, which is likely facilitated by the pure reconstruction objective that the model is trained with. However, GENESIS-V2 is the only model that separates foreground objects from the background in APC images. Environment conditions in Sketchy are highly controlled and SLOT-ATTENTION appears to be unable to handle the more complex conditions in APC images. Nevertheless, GENESIS-V2 also struggles to capture the fine-grained details and oversegments one of the foreground objects into several parts, leaving room for improvement in future work. Additional qualitative results are included in Appendix F.

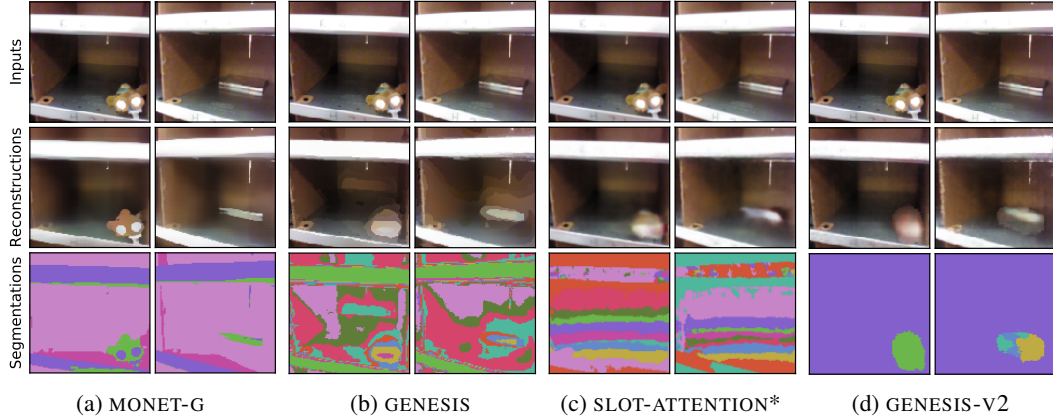


Figure 6: GENESIS-V2 is the only model that separates the foreground objects in images from APC.

Table 4: Segmentation metrics on APC.

	ARI	MSC
MONET-G	0.11	0.48
GENESIS	0.04	0.29
SLOT-ATT.	0.03	0.25
GENESIS-V2	0.55	0.67

Table 5: FID scores on Sketchy and APC.

	Sketchy	APC
MONET-G	294.3	269.3
GENESIS	241.9	183.2
SLOT-ATT.	—	—
GENESIS-V2	208.1	245.6

Table 4 reports the ARI and MSC scores computed from all pixels GENESIS-V2 and the baselines. GENESIS-V2 stands out in terms of both metrics, corroborating that GENESIS-V2 takes a valuable step towards learning unsupervised object-representations from *real-world* datasets. FID scores for generated images are summarised in Table 5 and qualitative results are included in Appendix F. GENESIS-V2 achieves the best FID on Sketchy, but it is outperformed by GENESIS on APC. Both models consistently outperform MONET-G. All of the FID scores, however, are fairly large which is not surprising given the much higher visual complexity of these images. It is therefore difficult to draw strong conclusions from these beyond a rough sense of sample quality. Further work is required to generate high-fidelity images after training on real-world datasets.

5 Conclusions

This work develops GENESIS-V2, a novel object-centric latent variable model of scenes which is able to both decompose visual scenes into semantically meaningful constituent parts while at the same time being able to generate coherent scenes in an object-centric fashion. GENESIS-V2 leverages a differentiable clustering algorithm for grouping pixel embeddings into a variable number of attention masks which are used to infer an unordered set of object representations. This approach is validated empirically on two established simulated datasets as well as two additional real-world datasets. The results show that GENESIS-V2 takes a step towards learning better object-centric representations without labelled supervision from real-world datasets.

In terms of future work, there is still room for improvement in terms of reconstruction, segmentation, and sample quality. It would also be interesting to investigate the ability of GENESIS-V2 and the IC-SBP to handle out-of-distribution images that contain more objects than seen during training. Moreover, several interesting variations of the IC-SBP were also already described in Section 3.1. Additional promising avenues include the extension of GENESIS-V2 to learn object representations from video (see e.g. [13, 14]) or to leverage recent advances in hierarchical latent variable models such as Nouveau VAEs (NVAEs) [61].

Acknowledgments and Disclosure of Funding

This research was supported by an EPSRC Programme Grant (EP/V000748/1) and a gift from Amazon Web Services (AWS). The authors would like to acknowledge the use of the University of Oxford Advanced Research Computing (ARC) facility in carrying out this work, <http://dx.doi.org/10.5281/zenodo.22558>, and the use of Hartree Centre resources. The Oxford Robotics Institute is supported by SCAN Computers in the form of hardware and services. Martin Engelcke was funded by an EPSRC DTA Studentship and a Google Studentship during his doctoral studies. Finally, the authors thank Yizhe Wu and Adam R. Kosiorek for useful comments and the NeurIPS reviewers for their time and feedback.

References

- [1] Andreas Geiger, Philip Lenz, and Raquel Urtasun. Are We Ready for Autonomous Driving? The KITTI Vision Benchmark Suite. In *IEEE/CVF Conference on Computer Vision and Pattern Recognition (CVPR)*, 2012.
- [2] Marius Cordts, Mohamed Omran, Sebastian Ramos, Timo Rehfeld, Markus Enzweiler, Rodrigo Benenson, Uwe Franke, Stefan Roth, and Bernt Schiele. The Cityscapes Dataset for Semantic Urban Scene Understanding. In *IEEE/CVF Conference on Computer Vision and Pattern Recognition (CVPR)*, 2016.
- [3] Coline Devin, Pieter Abbeel, Trevor Darrell, and Sergey Levine. Deep Object-Centric Representations for Generalizable Robot Learning. In *IEEE International Conference on Robotics and Automation (ICRA)*, 2018.
- [4] Shaoqing Ren, Kaiming He, Ross Girshick, and Jian Sun. Faster R-CNN: Towards Real-Time Object Detection with Region Proposal Networks. In *Advances in Neural Information Processing Systems (NeurIPS)*, 2015.
- [5] Kaiming He, Georgia Gkioxari, Piotr Dollár, and Ross Girshick. Mask R-CNN. In *International Conference on Computer Vision (ICCV)*, 2017.
- [6] Bohan Wu, Suraj Nair, Roberto Martin-Martin, Li Fei-Fei, and Chelsea Finn. Greedy Hierarchical Variational Autoencoders for Large-Scale Video Prediction. In *IEEE/CVF Conference on Computer Vision and Pattern Recognition (CVPR)*, 2021.
- [7] Jonathan Huang and Kevin Murphy. Efficient Inference in Occlusion-Aware Generative models of Images. *arXiv preprint arXiv:1511.06362*, 2015.
- [8] SM Ali Eslami, Nicolas Heess, Theophane Weber, Yuval Tassa, David Szepesvari, Geoffrey E Hinton, et al. Attend, Infer, Repeat: Fast Scene Understanding with Generative Models. In *Advances in Neural Information Processing Systems (NeurIPS)*, 2016.
- [9] Kun Xu, Chongxuan Li, Jun Zhu, and Bo Zhang. Multi-Objects Generation with Amortized Structural Regularization. In *Advances in Neural Information Processing Systems (NeurIPS)*, 2018.
- [10] Eric Crawford and Joelle Pineau. Spatially Invariant Unsupervised Object Detection with Convolutional Neural Networks. In *AAAI Conference on Artificial Intelligence*, 2019.
- [11] Jinyang Yuan, Bin Li, and Xiangyang Xue. Generative Modeling of Infinite Occluded Objects for Compositional Scene Representation. In *International Conference on Machine Learning (ICML)*, 2019.
- [12] Zhixuan Lin, Yi-Fu Wu, Skand Vishwanath Peri, Weihao Sun, Gautam Singh, Fei Deng, Jindong Jiang, and Sungjin Ahn. SPACE: Unsupervised Object-Oriented Scene Representation via Spatial Attention and Decomposition. In *International Conference on Learning Representations (ICLR)*, 2020.
- [13] Adam Kosiorek, Hyunjik Kim, Yee Whye Teh, and Ingmar Posner. Sequential Attend, Infer, Repeat: Generative Modelling of Moving Objects. In *Advances in Neural Information Processing Systems (NeurIPS)*, 2018.
- [14] Jindong Jiang, Sepehr Janghorbani, Gerard De Melo, and Sungjin Ahn. SCALOR: Generative World Models with Scalable Object Representations. In *International Conference on Learning Representations (ICLR)*, 2020.
- [15] Jindong Jiang and Sungjin Ahn. Generative Neurosymbolic Machines. In *Advances in Neural Information Processing Systems (NeurIPS)*, 2020.
- [16] Christopher P Burgess, Loic Matthey, Nicholas Watters, Rishabh Kabra, Irina Higgins, Matt Botvinick, and Alexander Lerchner. MONet: Unsupervised Scene Decomposition and Representation. *arXiv preprint arXiv:1901.11390*, 2019.
- [17] Martin Engelcke, Adam R Kosiorek, Oiwi Parker Jones, and Ingmar Posner. GENESIS: Generative Scene Inference and Sampling with Object-Centric Latent Representations. In *International Conference on Learning Representations (ICLR)*, 2020.

- [18] Martin Engelcke, Oiwi Parker Jones, and Ingmar Posner. Reconstruction Bottlenecks in Object-Centric Generative Models. *ICML Workshop on Object-Oriented Learning*, 2020.
- [19] Klaus Greff, Antti Rasmus, Mathias Berglund, Tele Hao, Harri Valpola, and Jürgen Schmidhuber. Tagger: Deep Unsupervised Perceptual Grouping. In *Advances in Neural Information Processing Systems (NeurIPS)*, 2016.
- [20] Klaus Greff, Sjoerd van Steenkiste, and Jürgen Schmidhuber. Neural Expectation Maximization. In *Advances in Neural Information Processing Systems (NeurIPS)*, 2017.
- [21] Sjoerd van Steenkiste, Michael Chang, Klaus Greff, and Jürgen Schmidhuber. Relational Neural Expectation Maximization: Unsupervised Discovery of Objects and their Interactions. In *International Conference on Learning Representations (ICLR)*, 2018.
- [22] Klaus Greff, Raphaël Lopez Kaufmann, Rishab Kabra, Nick Watters, Chris Burgess, Daniel Zoran, Loic Matthey, Matthew Botvinick, and Alexander Lerchner. Multi-Object Representation Learning with Iterative Variational Inference. In *International Conference on Machine Learning (ICML)*, 2019.
- [23] Rishi Veerapaneni, John D Co-Reyes, Michael Chang, Michael Janner, Chelsea Finn, Jiajun Wu, Joshua Tenenbaum, and Sergey Levine. Entity Abstraction in Visual Model-Based Reinforcement Learning. In *Conference on Robot Learning (CoRL)*, 2020.
- [24] Francesco Locatello, Dirk Weissenborn, Thomas Unterthiner, Aravindh Mahendran, Georg Heigold, Jakob Uszkoreit, Alexey Dosovitskiy, and Thomas Kipf. Object-Centric Learning with Slot Attention. In *Advances in Neural Information Processing Systems (NeurIPS)*, 2020.
- [25] Adam R Kosiorek, Sara Sabour, Yee Whye Teh, and Geoffrey E Hinton. Stacked Capsule Autoencoders. In *Advances in Neural Information Processing Systems (NeurIPS)*, 2019.
- [26] Yanchao Yang, Yutong Chen, and Stefano Soatto. Learning to Manipulate Individual Objects in an Image. In *IEEE/CVF Conference on Computer Vision and Pattern Recognition (CVPR)*, 2020.
- [27] Daniel M Bear, Chaofei Fan, Damian Mrowca, Yunzhu Li, Seth Alter, Aran Nayeibi, Jeremy Schwartz, Li Fei-Fei, Jiajun Wu, Joshua B Tenenbaum, et al. Learning Physical Graph Representations from Visual Scenes. In *Advances in Neural Information Processing Systems (NeurIPS)*, 2020.
- [28] Titas Anciukevicius, Christoph H Lampert, and Paul Henderson. Object-Centric Image Generation with Factored Depths, Locations, and Appearances. *arXiv preprint arXiv:2004.00642*, 2020.
- [29] Sjoerd van Steenkiste, Karol Kurach, and Sylvain Gelly. A Case for Object Compositionality in Deep Generative Models of Images. *NeurIPS Workshop on Modeling the Physical World: Learning, Perception, and Control*, 2018.
- [30] Mickaël Chen, Thierry Artières, and Ludovic Denoyer. Unsupervised Object Segmentation by Redrawing. In *Advances in Neural Information Processing Systems (NeurIPS)*, 2019.
- [31] Adam Bielski and Paolo Favaro. Emergence of Object Segmentation in Perturbed Generative Models. In *Advances in Neural Information Processing Systems (NeurIPS)*, 2019.
- [32] Relja Arandjelović and Andrew Zisserman. Object Discovery with a Copy-Pasting GAN. *arXiv preprint arXiv:1905.11369*, 2019.
- [33] Samaneh Azadi, Deepak Pathak, Sayna Ebrahimi, and Trevor Darrell. Compositional GAN: Learning Image-Conditional Binary Composition. *arXiv preprint arXiv:1807.07560*, 2019.
- [34] Thu Nguyen-Phuoc, Christian Richardt, Long Mai, Yong-Liang Yang, and Niloy Mitra. BlockGAN: Learning 3D Object-aware Scene Representations from Unlabelled Images. In *Advances in Neural Information Processing Systems (NeurIPS)*, 2020.
- [35] Sebastian Ehrhardt, Oliver Groth, Aron Monszpart, Martin Engelcke, Ingmar Posner, Niloy Mitra, and Andrea Vedaldi. RELATE: Physically Plausible Multi-Object Scene Synthesis Using Structured Latent Spaces. In *Advances in Neural Information Processing Systems (NeurIPS)*, 2020.
- [36] Michael Niemeyer and Andreas Geiger. GIRAFFE: Representing Scenes as Compositional Generative Neural Feature Fields. In *IEEE/CVF Conference on Computer Vision and Pattern Recognition (CVPR)*, 2020.
- [37] Diederik P Kingma and Max Welling. Auto-Encoding Variational Bayes. In *International Conference on Learning Representations (ICLR)*, 2014.
- [38] Danilo Jimenez Rezende, Shakir Mohamed, and Daan Wierstra. Stochastic Backpropagation and Approximate Inference in Deep Generative Models. In *International Conference on Machine Learning (ICML)*, 2014.
- [39] Max Jaderberg, Karen Simonyan, Andrew Zisserman, and Koray Kavukcuoglu. Spatial Transformer Networks. In *Advances in Neural Information Processing Systems (NeurIPS)*, 2015.
- [40] David Novotny, Samuel Albanie, Diane Larlus, and Andrea Vedaldi. Semi-Convolutional Operators for Instance Segmentation. In *European Conference on Computer Vision (ECCV)*, 2018.

- [41] Alireza Fathi, Zbigniew Wojna, Vivek Rathod, Peng Wang, Hyun Oh Song, Sergio Guadarrama, and Kevin P Murphy. Semantic Instance Segmentation via Deep Metric Learning. *arXiv preprint arXiv:1703.10277*, 2017.
- [42] Min Bai and Raquel Urtasun. Deep Watershed Transform for Instance Segmentation. In *IEEE/CVF Conference on Computer Vision and Pattern Recognition (CVPR)*, 2017.
- [43] Bert De Brabandere, Davy Neven, and Luc Van Gool. Semantic Instance Segmentation with a Discriminative Loss Function. *arXiv preprint arXiv:1708.02551*, 2017.
- [44] Rishabh Kabra, Chris Burgess, Loic Matthey, Raphael Lopez Kaufman, Klaus Greff, Malcolm Reynolds, and Alexander Lerchner. Multi-Object Datasets, 2019. URL <https://github.com/deepmind/multi-object-datasets/>.
- [45] Oliver Groth, Fabian B Fuchs, Ingmar Posner, and Andrea Vedaldi. ShapeStacks: Learning Vision-Based Physical Intuition for Generalised Object Stacking. In *European Conference on Computer Vision (ECCV)*, 2018.
- [46] Serkan Cabi, Sergio Gómez Colmenarejo, Alexander Novikov, Ksenia Konyushkova, Scott Reed, Rae Jeong, Konrad Zolna, Yusuf Aytar, David Budden, Mel Vecerik, et al. Scaling Data-Driven Robotics with Reward Sketching and Batch Reinforcement Learning. In *Robotics: Science and Systems (RSS)*, 2020.
- [47] Andy Zeng, Kuan-Ting Yu, Shuran Song, Daniel Suo, Ed Walker Jr, Alberto Rodriguez, and Jianxiong Xiao. Multi-view Self-supervised Deep Learning for 6D Pose Estimation in the Amazon Picking Challenge. In *IEEE International Conference on Robotics and Automation (ICRA)*, 2017.
- [48] Ian Goodfellow, Jean Pouget-Abadie, Mehdi Mirza, Bing Xu, David Warde-Farley, Sherjil Ozair, Aaron Courville, and Yoshua Bengio. Generative Adversarial Nets. In *Advances in Neural Information Processing Systems (NeurIPS)*, 2014.
- [49] Andrew Brock, Jeff Donahue, and Karen Simonyan. Large Scale GAN Training for High Fidelity Natural Image Synthesis. In *International Conference on Learning Representations (ICLR)*, 2019.
- [50] Klaus Greff, Sjoerd van Steenkiste, and Jürgen Schmidhuber. On the Binding Problem in Artificial Neural Networks. *arXiv preprint arXiv:2012.05208*, 2020.
- [51] Yan Zhang, Jonathon Hare, and Adam Prügel-Bennett. Deep Set Prediction Networks. In *Advances in Neural Information Processing Systems (NeurIPS)*, 2019.
- [52] Eric Nalisnick and Padhraic Smyth. Stick-Breaking Variational Autoencoders. In *International Conference on Learning Representations (ICLR)*, 2017.
- [53] Manzil Zaheer, Satwik Kottur, Siamak Ravanbakhsh, Barnabas Poczos, Ruslan Salakhutdinov, and Alexander Smola. Deep Sets. In *Advances in Neural Information Processing Systems (NeurIPS)*, 2017.
- [54] Edward Wagstaff, Fabian Fuchs, Martin Engelcke, Ingmar Posner, and Michael A Osborne. On the Limitations of Representing Functions on Sets. In *International Conference on Machine Learning (ICML)*, 2019.
- [55] Shu Kong and Charless C Fowlkes. Recurrent Pixel Embedding for Instance Grouping. In *IEEE/CVF Conference on Computer Vision and Pattern Recognition (CVPR)*, 2018.
- [56] Danilo Jimenez Rezende and Fabio Viola. Taming VAEs. *arXiv preprint arXiv:1810.00597*, 2018.
- [57] Lawrence Hubert and Phipps Arabie. Comparing Partitions. *Journal of Classification*, 2(1):193–218, 1985.
- [58] Pablo Arbelaez, Michael Maire, Charless Fowlkes, and Jitendra Malik. Contour Detection and Hierarchical Image Segmentation. *IEEE Transactions on Pattern Analysis and Machine Intelligence*, 33(5), 2010.
- [59] Martin Heusel, Hubert Ramsauer, Thomas Unterthiner, Bernhard Nessler, and Sepp Hochreiter. GANs Trained by a Two Time-Scale Update Rule Converge to a Local Nash Equilibrium. In *Advances in Neural Information Processing Systems (NeurIPS)*, 2017.
- [60] Maximilian Seitzer. pytorch-fid: FID Score for PyTorch. <https://github.com/mseitzer/pytorch-fid>, August 2020. Version 0.1.1.
- [61] Arash Vahdat and Jan Kautz. NVAE: A Deep Hierarchical Variational Autoencoder. In *Advances in Neural Information Processing Systems (NeurIPS)*, 2020.
- [62] Olaf Ronneberger, Philipp Fischer, and Thomas Brox. U-Net: Convolutional Networks for Biomedical Image Segmentation. In *International Conference on Medical Image Computing and Computer-Assisted Intervention (MICCAI)*, 2015.
- [63] Dmitry Ulyanov, Andrea Vedaldi, and Victor Lempitsky. Instance Normalization: The Missing Ingredient for Fast Stylization. *arXiv preprint arXiv:1607.08022*, 2016.
- [64] Yuxin Wu and Kaiming He. Group Normalization. In *European Conference on Computer Vision (ECCV)*, 2018.

- [65] Jimmy Lei Ba, Jamie Ryan Kiros, and Geoffrey E Hinton. Layer Normalization. *arXiv preprint arXiv:1607.06450*, 2016.
- [66] Nicholas Watters, Loic Matthey, Christopher P Burgess, and Alexander Lerchner. Spatial Broadcast Decoder: A Simple Architecture for Learning Disentangled Representations in VAEs. *ICLR Workshop on Learning from Limited Data*, 2019.
- [67] Sepp Hochreiter and Jürgen Schmidhuber. Long Short-Term Memory. *Neural Computation*, 1997.
- [68] Diederik P Kingma and Jimmy Ba. Adam: A Method for Stochastic Optimization. In *International Conference on Learning Representations (ICLR)*, 2015.
- [69] Adam Paszke, Sam Gross, Soumith Chintala, Gregory Chanan, Edward Yang, Zachary DeVito, Zeming Lin, Alban Desmaison, Luca Antiga, and Adam Lerer. Automatic Differentiation in PyTorch. 2017.

A Graphical Models

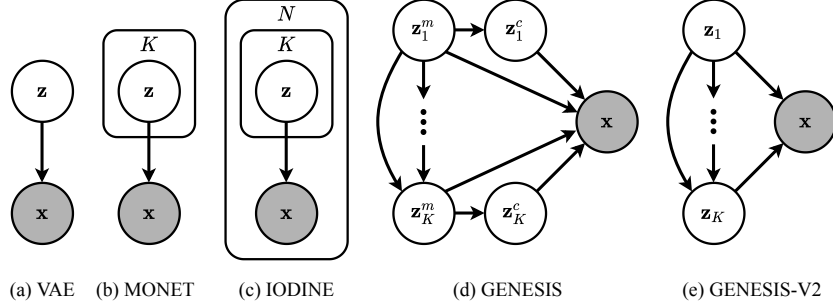


Figure 7: Graphical model of GENESIS-V2 compared to a standard VAE [37, 38], MONET [16], IODINE [22], and GENESIS [17]. N denotes the number of refinement iterations in IODINE. GENESIS and GENESIS-V2 capture correlations between object slots with an autoregressive prior.

B GENESIS-V2 Architecture Details

The GENESIS-V2 architecture consists of four main components: a deterministic backbone, the attention and object pooling module, the component decoders, and an optional autoregressive prior which are described in detail below.

Backbone GENESIS-V2 uses a UNet [62] encoder similar to the attention network in the re-implementation of MONET in Engelcke et al. [17] with [64, 64, 128, 128, 128] filters in the encoder and the reverse in the decoder. Each convolutional block decreases or increases the spatial resolution by a factor of two and there are two hidden layers with 128 units each in between the encoder and the decoder. The only difference to the UNet implementation in Engelcke et al. [17] is that the instance normalisation (IN) layers [63] are replaced with group normalisation (GN) layers [64] to preserve contrast information. The number of groups is set to eight in all such layers which is also referred to as a GN8 layer. The output of this backbone encoder is a feature map $\mathbf{e} \in \mathbb{R}^{H \times W \times D_e}$ with $D_e = 64$ output channels and spatial dimensions that are equal to the height and width of the input image.

Attention and Object Pooling Following feature extraction, an *attention head* computes pixel-wise semi-convolutional embeddings ζ with eight channels, i.e. $D_\zeta = 8$, as in Novotny et al. [40]. The attention head consists of a 3×3 Conv-GN8-ReLU block with 64 filters and a 1×1 semi-convolutional layer. The pixel embeddings are clustered into K attention masks $\mathbf{m}_{1:K}$ using the IC-SBP. A Gaussian kernel ψ_G is used unless noted otherwise. A *feature head* consisting of a 3×3 Conv-GN8-ReLU block with 64 filters and a 1×1 convolution with 128 filters refines the encoder output \mathbf{e} to obtain a new feature map $\mathbf{f} \in \mathbb{R}^{H \times W \times D_f}$ with $D_f = 128$. Similar to Locatello et al. [24], the attention masks $\mathbf{m}_{1:K}$ are used to pool feature vectors from the feature map by multiplying the feature map with an individual attention mask and summing across the spatial dimensions. Each pooled feature vector is normalised by dividing by the sum of the attention mask values plus a small epsilon value to avoid numerical instabilities. Finally, a *posterior head* uses layer normalisation [65] followed by a fully-connected ReLU block with 128 units and a second fully-connected layer to compute the sufficient statistics of the individual object latents $\mathbf{z}_{1:K}$ with $\mathbf{z}_k \in \mathbb{R}^{64}$ from pooled feature vector.

Component Decoders Following Greff et al. [22] and Locatello et al. [24], the object latents are decoded by separate decoders with shared weights to parameterise the sufficient statistics of the SGMM in Equation (1). Each decoded component has four channels per pixel. The first three channels contain the RGB values and the fourth channel contains the unnormalised segmentation logits which are normalised across scene components using a softmax operator. Again following Locatello et al. [24], the first layer is a spatial broadcasting module as introduced in Watters et al. [66] which is designed to facilitate the disentanglement of the independent factors of variation in a dataset. An additional advantage of spatial broadcasting is that it requires a smaller number of parameters than a fully-connected layer when upsampling a feature vector to a specific spatial resolution. The

spatial broadcasting module is followed by four 5×5 , stride-2 deconvolutional GN8-ReLU layers with 64 filters to retrieve the full image resolution before a final 1×1 convolution which computes the four output channels. The use of stride-2 deconvolutional layers should make the GENESIS-V2 decoder more flexible compared to the counterparts used in MONET-G and GENESIS, which broadcast higher resolution and use stride-1 convolutions for decoding (see also [18]).

Autoregressive Prior Identical to GENESIS [17], the autoregressive prior for scene generation is implemented as an LSTM [67] followed by a fully-connected linear layer with 256 units to infer the sufficient statistics of the prior distribution for each component.

C Kernel Initialisation

Assume a maximum of K scene components to be present in an image and that model is initialised so that the pixel embeddings are equal to the relative pixel coordinates with the other dimensions being zero at the beginning of training. For each initial mask to cover approximately the same area of an image, further assume that the circular isocontours of the kernels are packed into an image in a square fashion. Using linear relative pixel coordinates in $[-1, 1]$ and dividing an image into K equally sized squares, each square has a side-length of $2/\sqrt{K}$. Let the mask value decrease to 0.5 at the intersection of the square and the circular isocontour, i.e., at a distance of $1/\sqrt{K}$ from the centre of the kernel as illustrated in Figure 8. Solving this for each kernel in Equation (3) leads to

$$\psi\left(0, 1/\sqrt{K}\right) = 0.5 \iff \sigma_G^{-1} = K \ln 2, \quad \sigma_L^{-1} = \sqrt{K} \ln 2, \quad \sigma_E^{-1} = K/2. \quad (8)$$

Examples of the initial masks obtained when running the IC-SBP with the proposed initialisations are illustrated in Figure 9.

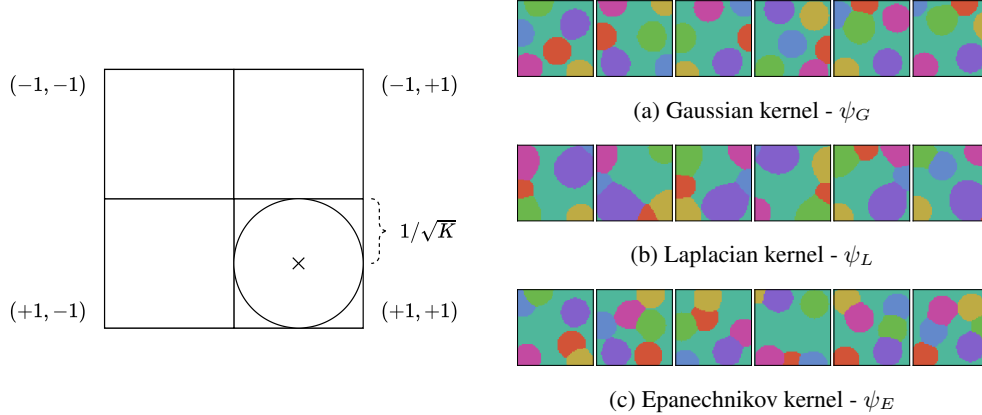


Figure 8: Illustration of packing $K = 4$ circular kernels into a square image and linear relative pixel coordinates in $[-1, 1]$, resulting in circular isocontours of radius $1/\sqrt{K}$.

Figure 9: Initial masks obtained when running the IC-SBP with different randomly sampled seed scores, using the initialisations in Equation (8) and $K = 7$.

D Datasets

We evaluate GENESIS-V2 on simulated images from ObjectsRoom [44] and ShapeStacks [45] as well as real-world images from Sketchy [46] and APC [47]. ObjectsRoom and ShapeStacks are well established in the context of this work and we follow the same preprocessing procedures as used in Engelcke et al. [17] and Engelcke et al. [18]. As in these works, the default number of object slots is set to $K = 7$ and $K = 9$ for ObjectsRoom and ShapeStacks, respectively, across all models. This work is the first to train and evaluate models that aim to learn object representations without supervision on Sketchy and APC. We therefore developed our own preprocessing and training/validation/test splits, which are described in detail below. The exact splits that were used will be released along with the code for reproducibility.

Sketchy The Sketchy dataset [46] is designed for off-policy reinforcement learning (RL), providing episodes showing a robotic arm performing different tasks that involve three differently coloured shapes (blue, red, green) or a cloth. The dataset includes camera images from several viewpoints, depth images, manipulator joint information, rewards, and other meta-data. The dataset is quite considerable in size and takes about 5TB of storage in total. We ease the computational and storage demands by only using a subset of this dataset. Specifically, we use the high-quality demonstrations from the “lift-green” and “stack-green-on-red” tasks corresponding to a total of 395 episodes, 10% of which are set aside as validation and test sets each. Sketchy also contains episodes from a task that involves lifting a cloth and an even larger number of lower-quality demonstrations that offer a wider coverage of the state space. We restrict ourselves to the high-quality episodes that involve the manipulation of solid objects. The number of high-quality episodes alone is already considerable and we want to evaluate whether the models can separate multiple foreground objects. From these episodes, we use the images from the front-left and front-right cameras which show the arm and the foreground objects without obstruction.

The raw images have a resolution of 600-by-960 pixels. To remove uninteresting pixels belonging to the background, 144 pixels on the left and right are cropped away for both camera views, the top 71 and bottom 81 pixels are cropped away for the front-left view, and the top 91 and bottom 61 are cropped away for the front-right view, resulting in a 448-by-672 crop. From this 448-by-672 crop, seven square crops are extracted to obtain a variety of views for the models to learn from. The first crop corresponds to the centre 448-by-448 pixels. For the other six crops, the top and bottom left, centre, and right squares of size 352 are extracted. Finally, we resize these crops to a resolution of 128-by-128 to reduce the computational demands of training the models. This leads to a total of 337,498 training; 41,426 validation; and 41,426 test images. Examples of images obtained with this preprocessing procedure are shown in Figure 10. The default number of object slots is set to $K = 10$ across all models to give them sufficient flexibility to discover different types of solutions.

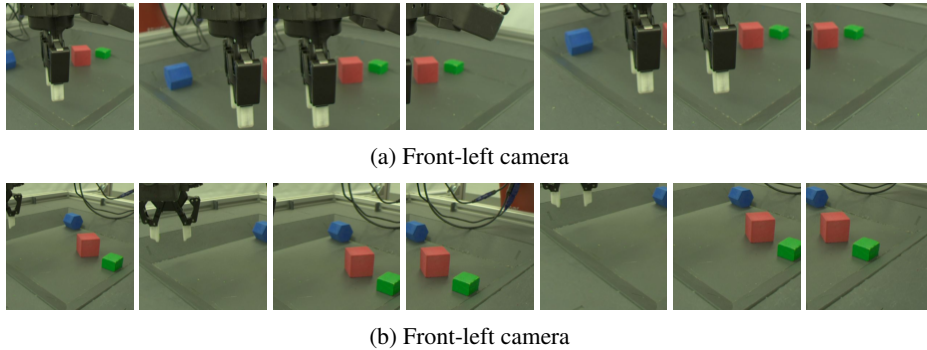


Figure 10: 128-by-128 crops as used for training, extracted from the front-left and front-right cameras of a single image from the Sketchy dataset [46]. Showing from left to right: centre, top-left, top-centre, top-right, bottom-left, bottom-centre, and bottom-right crops.

APC For their entry to the 2016 Amazon Picking Challenge (APC), the MIT-Princeton team created and released an object segmentation training set, showing a single challenge object either on a shelf or in a tray [47]. The raw images are first resized so that the shorter image side has a length of 128 pixels. The centre 128-by-128 pixels are then extracted to remove uninteresting pixels belonging to the background. Example images after processing are shown in Figure 11. For each object, there exists a set of scenes showing the object in different poses on both the shelf and in the red tray. For each scene, there are images taken from different camera viewpoints. We select 10% of the scenes at random to be set aside for validation and testing each so that scenes between the training, validation, and test sets do not overlap. The resulting training, validation, and test sets consist of 109,281; 13,644; and 13,650 images, respectively. As for Sketchy, the default number of object slots is set to $K = 10$ to provide enough flexibility for models to discover different types of solutions.

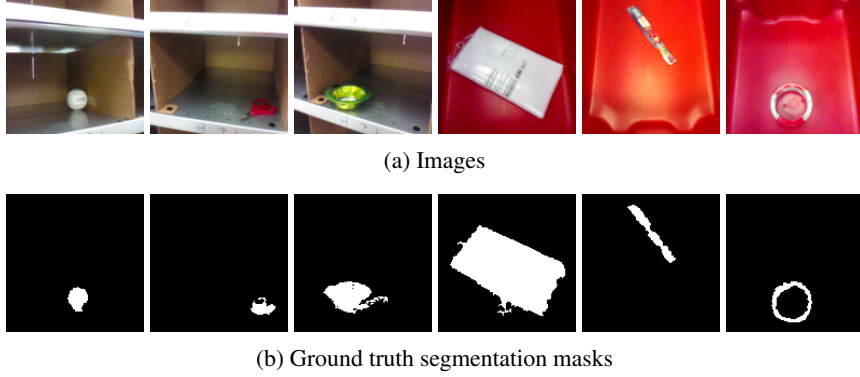


Figure 11: Examples from the APC dataset [47] after cropping and resizing.

E Training Details

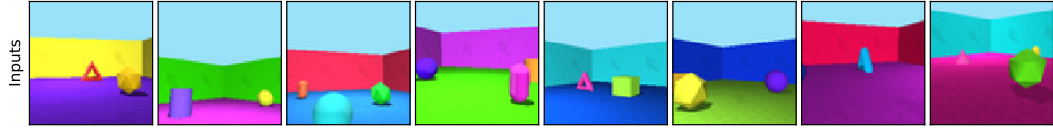
Models apart from SLOT-ATTENTION are trained with the protocol from Engelcke et al. [17] for comparability, which minimises the GECO objective [56] using the Adam optimiser [68], a learning rate of 10^{-4} , a batch size of 32, and 500,000 training iterations. The Gaussian standard deviation σ_x in Equation (1) is set to 0.7 and GECO reconstruction goal is set to a negative log-likelihood value per pixel and per channel of 0.5655 for the simulated datasets and the APC dataset. For Sketchy, a GECO goal of 0.5645 was found to lead to better segmentations and was used instead. As in Engelcke et al. [17], the GECO hyperparameters are set to $\alpha_g = 0.99$, $\eta = 10^{-5}$ when $C \leq E$ and $\eta = 10^{-4}$ otherwise. β_g is initialised to 1.0 and clamped to a minimum value of 10^{-10} . For experiments with the auxiliary mask consistency loss in Equation (7), we found that an initial high weighting of the mask loss inhibits the learning of good segmentations, so in these experiments β_g is initialised to 10^{-10} instead. We refer to MONET trained with GECO as MONET-G to avoid conflating the results with the original settings from Burgess et al. [16]. SLOT-ATTENTION is trained using the official reference implementation with default hyperparameters. Training on 64-by-64 images from ObjectsRoom and ShapeStacks takes around two days with a single NVIDIA Titan RTX GPU. Similarly, training on 128-by-128 images from Sketchy and APC takes around eight days.

F Additional results

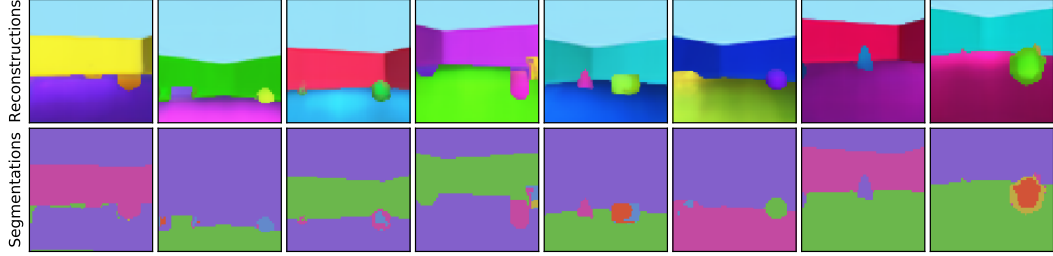
Table 6 shows a set of ablations for GENESIS-V2 in terms of segmentation performance. A first set of experiments is conducted with an independent prior, the three different distance kernels described in Section 3.2, and semi-convolutional embeddings. The Gaussian kernel appears to perform most robustly and is therefore selected for all other experiments. A second set of experiments is conducted in which models are trained with an auto-regressive prior and either with a semi-convolutional or a standard convolutional output layer for obtaining pixel embeddings. Both the auto-regressive prior and the semi-convolutional operation improve segmentation performance.

Table 6: GENESIS-V2 ablations showing means and standard deviations from three seeds. Highlighting follows an analogous scheme as in Table 1.

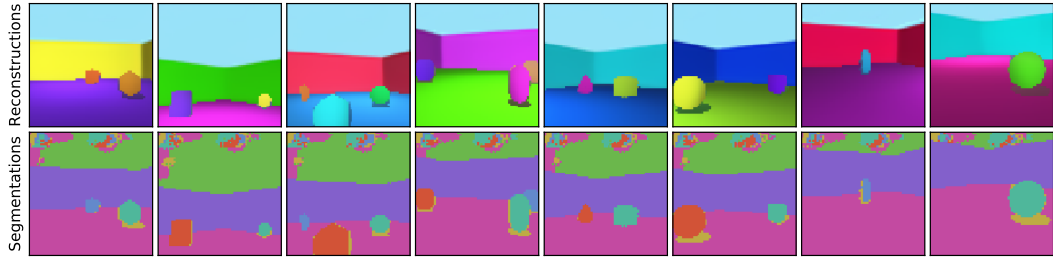
Auto-reg. prior	Kernel	Semi-conv.	ObjectsRoom		ShapeStacks	
			ARI-FG	MSC-FG	ARI-FG	MSC-FG
No	ψ_G	Yes	0.79±0.01	0.47±0.17	0.79±0.01	0.67±0.00
No	ψ_L	Yes	0.74±0.08	0.48±0.20	0.79±0.01	0.67±0.01
No	ψ_E	Yes	0.78±0.01	0.34±0.08	0.78±0.01	0.66±0.01
Yes	ψ_G	Yes	0.84±0.01	0.58±0.03	0.81±0.00	0.68±0.01
Yes	ψ_G	No	0.79±0.05	0.59±0.02	0.60±0.38	0.56±0.21



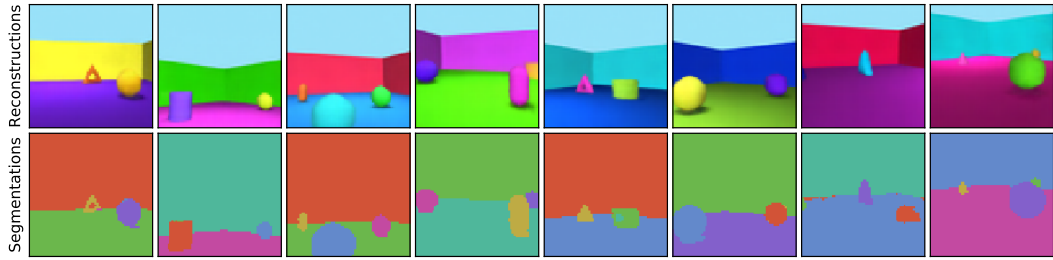
(a) Input images



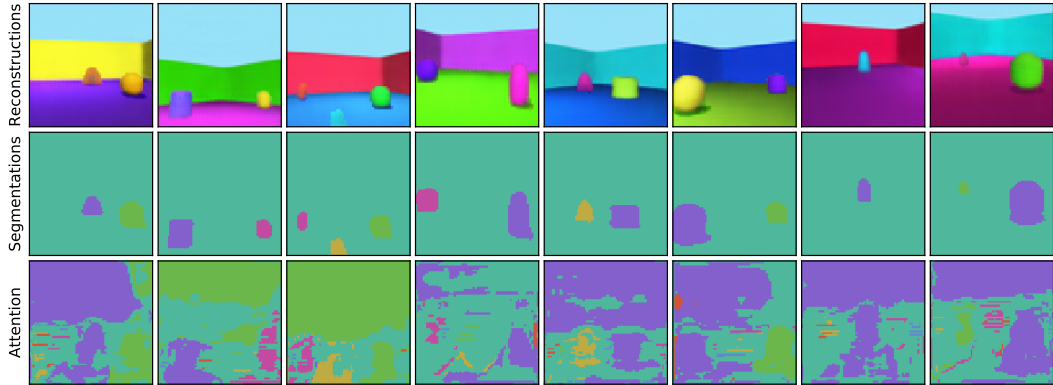
(b) MONET-G



(c) GENESIS

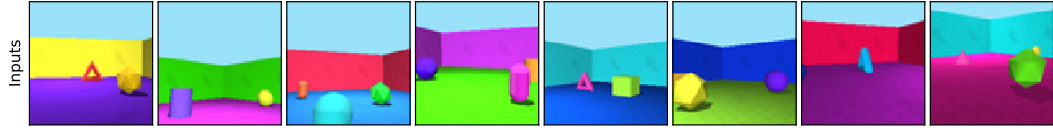


(d) SLOT-ATTENTION

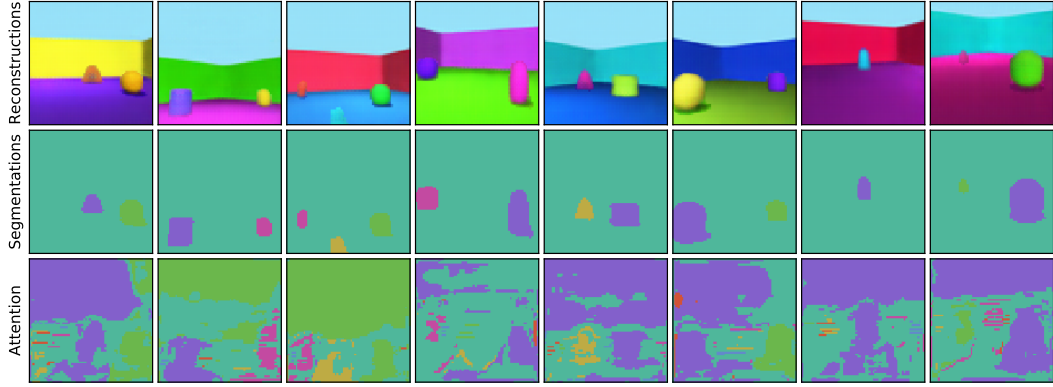


(e) GENESIS-V2

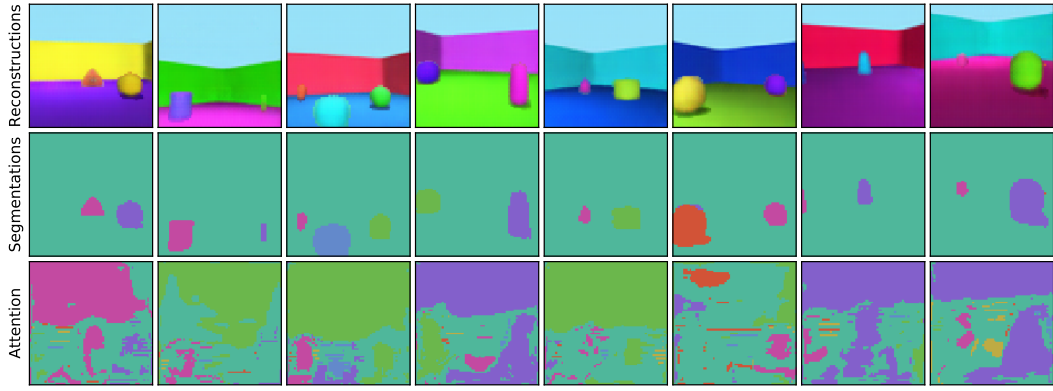
Figure 12: ObjectsRoom reconstructions and segmentations.



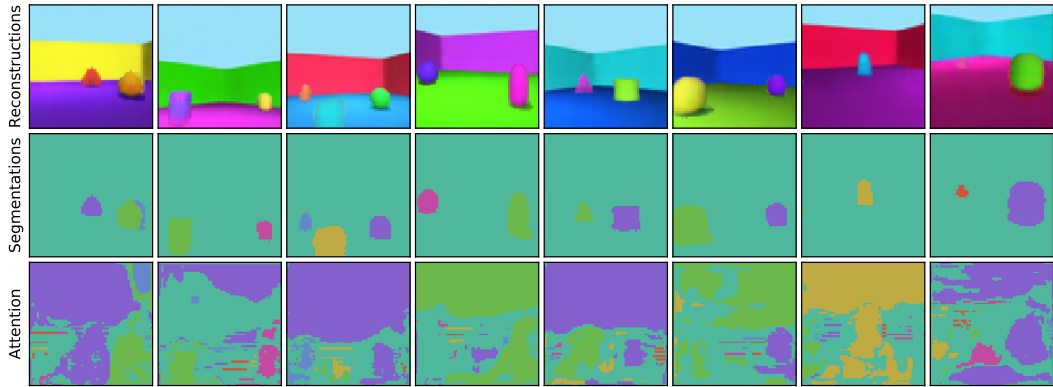
(a) Input images



(b) First random seed



(c) Second random seed



(d) Third random seed

Figure 13: Applying GENESIS-V2 several times to the same images from the ObjectsRoom dataset with three different random seeds shows that the model produces similar reconstructions and segmentations for each seed, but foreground objects are allocated to different slots as indicated by the segmentation colours.

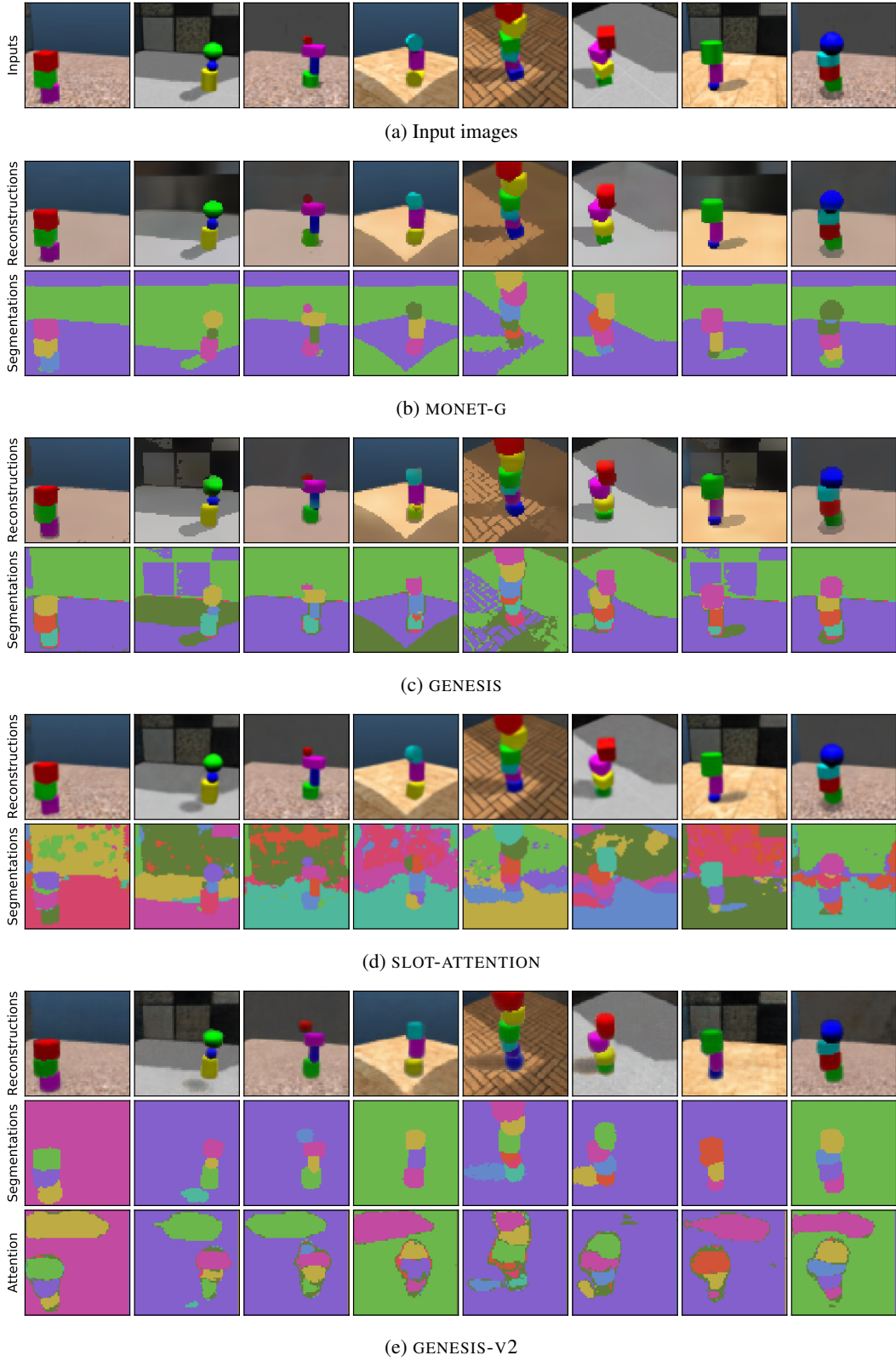
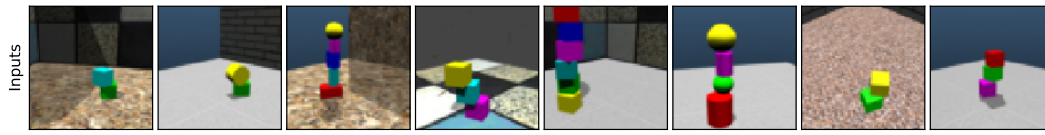
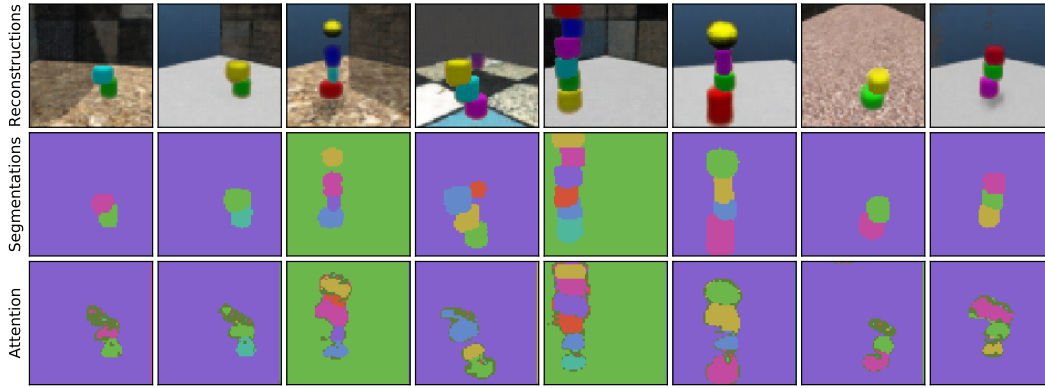


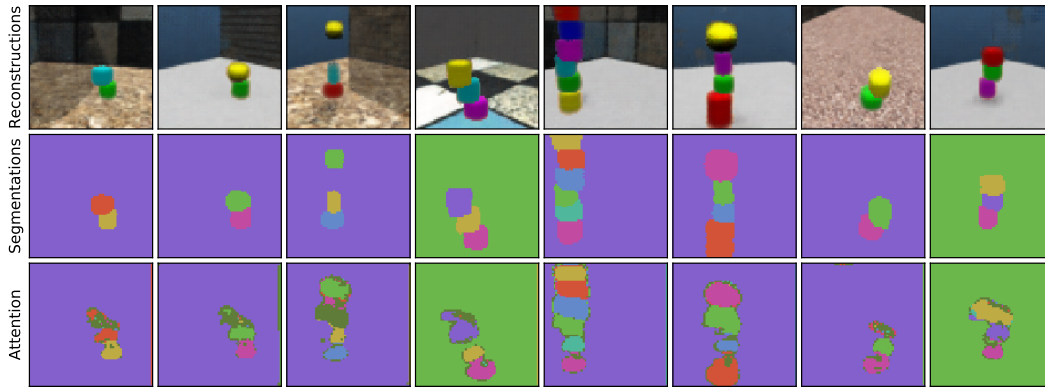
Figure 14: ShapeStacks reconstructions and segmentations.



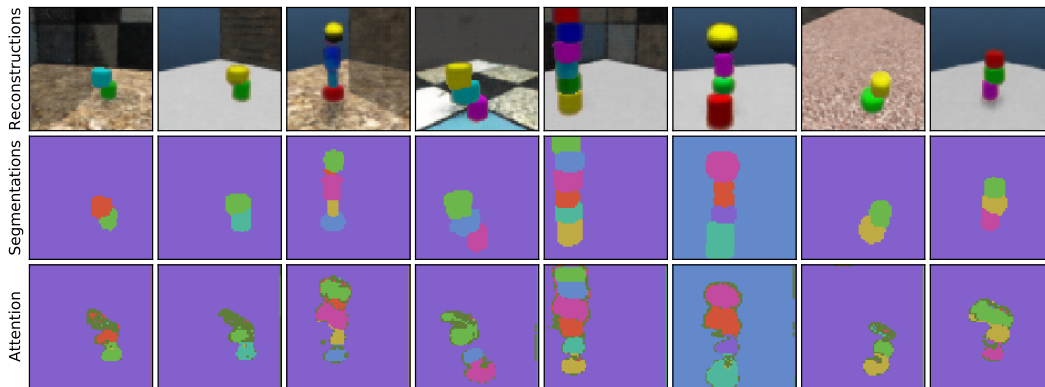
(a) Input images



(b) First random seed

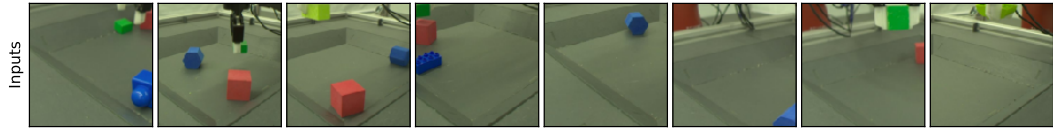


(c) Second random seed

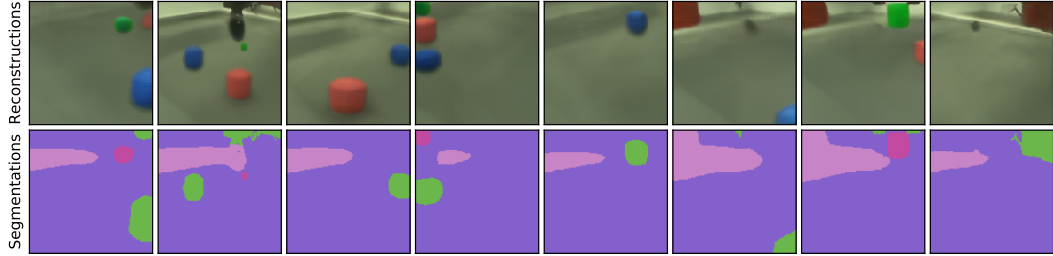


(d) Third random seed

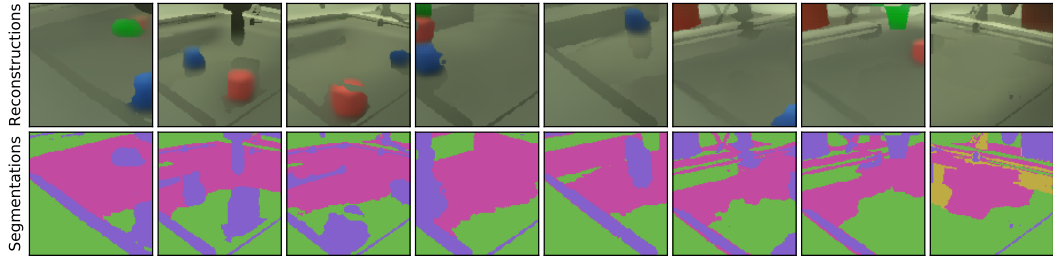
Figure 15: Applying GENESIS-V2 several times to the same images from the ShapeStacks dataset with three different random seeds shows that the model produces similar reconstructions and segmentations for each seed, but components are allocated to different slots as indicated by the segmentation colours.



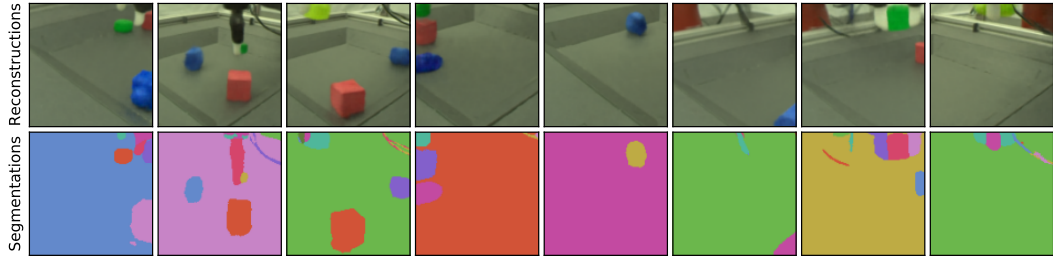
(a) Input images



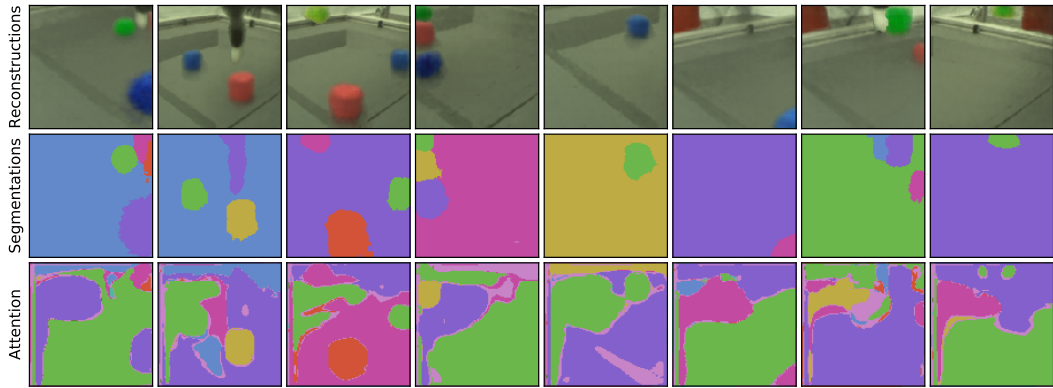
(b) MONET-G



(c) GENESIS



(d) SLOT-ATTENTION



(e) GENESIS-V2

Figure 16: Sketchy reconstructions and segmentations.

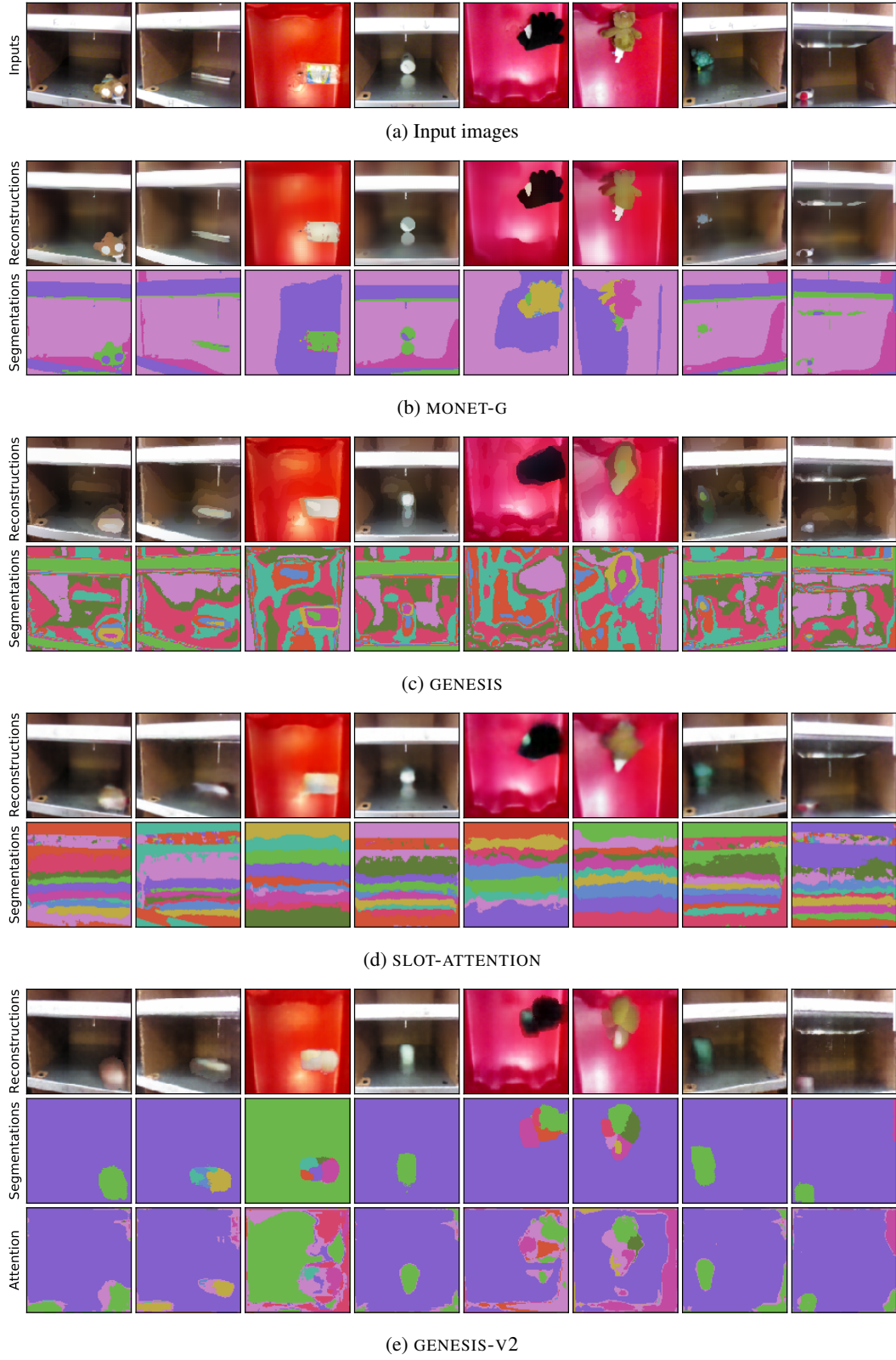
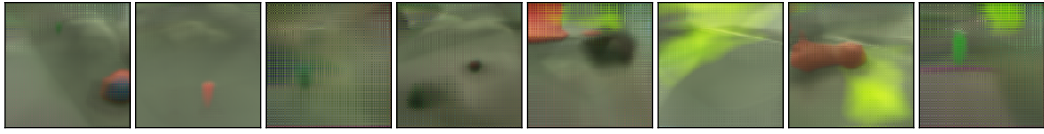
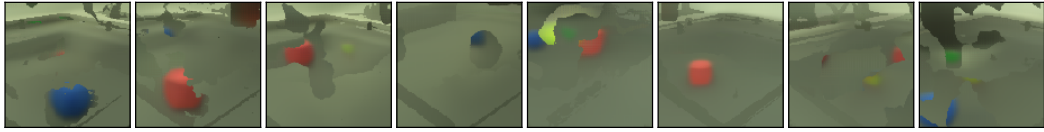


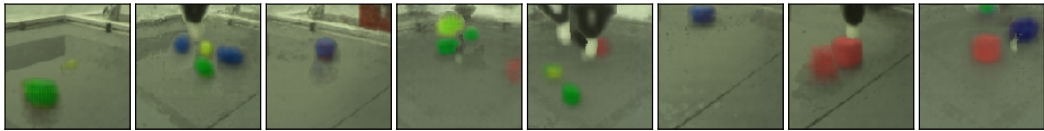
Figure 17: APC reconstructions and segmentations.



(a) MONET-G

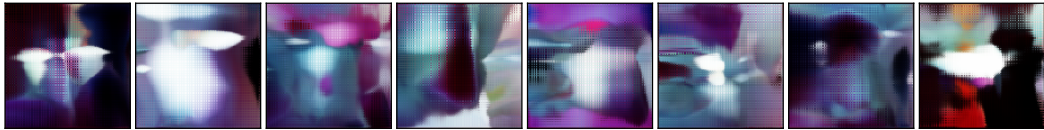


(b) GENESIS

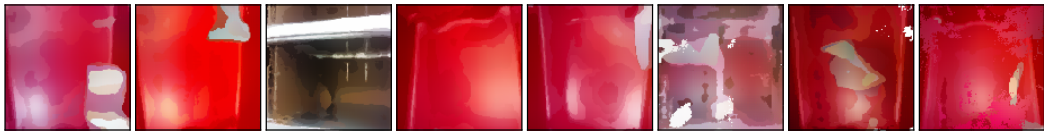


(c) GENESIS-V2

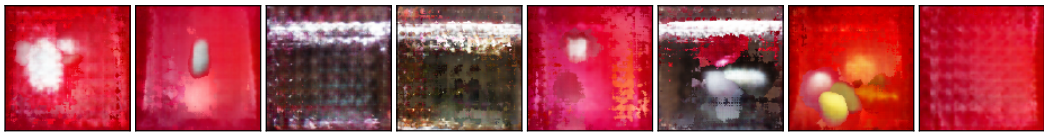
Figure 18: Sketchy samples.



(a) MONET-G



(b) GENESIS



(c) GENESIS-V2

Figure 19: APC samples.

G Potential Negative Societal Impacts

GENESIS-V2 is a generative model. Generative models can potentially be used spread disinformation by generating synthetic images for manipulative purposes. At this point in time, however, GENESIS-V2 is only able to generate plausible images when training on simulated images with limited visual complexity. A direct application of this method for malicious purposes is therefore unlikely.

H Third-Party Assets

GENESIS-V2 is implemented using PyTorch [69]. In addition to various Python packages, we make use of several third-party assets:

- Kabra et al. [44] (Apache-2.0 License): ObjectsRoom dataset,
- Groth et al. [45] (GPL-3.0 License): ShapeStacks dataset,
- Cabi et al. [46] (Apache-2.0 License): Sketchy dataset,
- Zeng et al. [47] (BSD-2-Clause License): APC dataset,
- Engelcke et al. [17, 18] (GPL-3.0 License): Implementation of GENESIS and MONET-G,
- Locatello et al. [24] (Apache-2.0 License): Implementation of SLOT-ATTENTION,
- Seitzer [60] (Apache-2.0 License): FID computation in PyTorch.

The datasets are publicly available under open-source licenses and consent was therefore not explicitly requested. To the best of our knowledge, none of the datasets contain personally identifiable information or offensive content.